The Astronomical Journal, 129:2294–2307, 2005 May

A SEARCH FOR SUBSTELLAR COMPANIONS AROUND 15 WEAK-LINED T TAURI STARS WITH THE PLANETARY CAMERA 2 OF THE *HUBBLE SPACE TELESCOPE*[1,2]

Alessandro Massarotti
Harvard-Smithsonian Center for Astrophysics, 60 Garden Street, Cambridge, MA 02138; and Department of Physics and Astronomy, Stonehill College, 320 Washington Street, Easton, MA 02357; amassaro@cfa.harvard.edu

David W. Latham and Guillermo Torres
Harvard-Smithsonian Center for Astrophysics, 60 Garden Street, Cambridge, MA 02138; dlatham@cfa.harvard.edu, gtorres@cfa.harvard.edu

Robert A. Brown
Space Telescope Science Institute, 3700 San Martin Drive, Baltimore, MD 21218; rbrown@stsci.edu

and

Benjamin D. Oppenheimer
Department of Astronomy, Harvard University, 60 Garden Street, Cambridge, MA 02138;[3] boppenheimer@as.arizona.edu

Received 2004 March 11; accepted 2005 January 26

ABSTRACT

To search for thermal emission from substellar companions, we have obtained *Z*-band images of 15 weak-lined T Tauri stars in the Taurus-Auriga and Ophiuchus star-forming regions using the Planetary Camera 2 on the *Hubble Space Telescope*. We found 18 faint nearby objects at separations larger than 4″ but none at smaller separations. For 11 of these we have enough color information to suggest that they are not substellar members of the star-forming regions. The remaining seven faint nearby objects are candidate substellar objects. Our detection limit for companions with separations larger than about 1″ is apparent $Z = 19.5$ mag, corresponding to substellar objects in the mass range $3M_J$–$15M_J$ for the age range of our targets, 1.2–25 Myr. Our detection limit degrades for smaller separations and is 4–6 mag poorer at a separation of 0.″2, corresponding to a projected separation of 30 AU. Inside 0.″2 our sensitivity is insufficient to detect substellar companions. To complement the imaging program, extensive spectroscopic observations were obtained with the Center for Astrophysics Digital Speedometers. Four of our targets proved to be spectroscopic binaries, one of them double-lined. We report orbital solutions for these four stars. Our radial velocities support the membership of all our targets to their respective star-forming regions, except for HD 283759, which must be rejected as a member.

Key words: binaries: spectroscopic — planetary systems — stars: imaging — stars: low-mass, brown dwarfs — stars: pre–main-sequence

1. INTRODUCTION

Diffraction-limited imaging with the *Hubble Space Telescope* (*HST*) offers the opportunity to search for faint low-mass companions of young stellar objects in a new circumstellar domain not yet accessible to either the Doppler or astrometric approaches, namely for angular separations larger than about 0.″2. In this domain the acceleration of a star induced by a low-mass companion is too small to be detected by the two classical indirect techniques. In this paper we report the results of a search for thermal emission from substellar companions around 15 weak-lined T Tauri stars (WTTSs) in the Taurus-Auriga and Ophiuchus star-forming regions using the *Z* band with the Planetary Camera 2 (PC2) on *HST*.

The two main factors controlling the thermal emission from substellar companions more than a few AU away from their parent stars are their mass and age. Objects more massive than about $12M_J$ can briefly burn deuterium, but ultimately all objects below about $80M_J$ radiate away the energy derived from gravitational contraction and must therefore cool and fade (Burrows et al. 1997). Therefore, the main strategy of our search for substellar companions is to look for them around young stars using deep imaging, before they have had time to cool and grow too faint to be detected.

When direct imaging is used, targets that are closer to us are better, because that allows us to probe to smaller orbital sizes and fainter companions. Unfortunately, there are very few stars in the nearby field that are young enough for this experiment, say less than 5 Myr old. Furthermore, the ages of young field stars are difficult to establish if their distances are poorly determined. For these reasons we have chosen to observe stars in two of the nearest star-forming regions, Taurus-Auriga and Ophiuchus, where there are many stars younger than 10^7 yr, and the ages can be estimated from the observed luminosities and spectral types under the assumption that all the targets belong to the same physical association and are at the same distance. The main disadvantage of observing targets in the Taurus-Auriga and Ophiuchus

[1] Some of the results presented here used observations made with the MMT, a joint facility of the Smithsonian Institution and the University of Arizona.

[2] This publication makes use of data products from the Two Micron All Sky Survey (2MASS), which is a joint project of the University of Massachusetts and the Infrared Processing and Analysis Center/California Institute of Technology, funded by the National Aeronautics and Space Administration and the National Science Foundation (NSF).

[3] Current address: Department of Astronomy, Steward Observatory, University of Arizona, 933 North Cherry Avenue, Tucson, AZ 85721-0065.

TABLE 1
TARGET WEAK-LINED T TAURI STARS

Star	R.A. (J2000)	Decl. (J2000)	V	$B-V$	$K-L$	$W(\mathrm{H}\alpha)$	A_Z	Spectral Type	log $T_{\rm eff}$	log $(L/L_\odot)$	Ref.
HBC 374	04 18 47.04	+28 20 07.3	12.67	1.68	0.01	+3.0	0.32	K7	3.61	+0.18	1
HBC 376	04 18 51.70	+17 23 16.6	12.28	1.13	0.11	+0.7	0.00	K7	3.61	−0.42	1
HBC 397	04 32 09.27	+17 57 22.8	12.06	1.23	0.04	+0.5	0.29	K7	3.61	−0.30	1
HBC 399	04 32 14.57	+18 20 14.7	12.27	1.41	0.10	+1.8	0.12	K7	3.61	−0.10	1
HBC 400a	04 32 15.84	+18 01 38.7	12.11	1.39	0.18	+1.6	0.12	K7	3.61	−0.28	1
HBC 400b							0.12	K7	3.61	−0.40	1
HD 283759	04 36 48.21	+24 12 58.8	10.36	0.76	0.00			F5	3.81	+0.61	2, 3
HBC 419	04 39 17.80	+22 21 03.5	12.41	1.37	0.57	+12.7	0.26	K5	3.64	−0.08	1
HBC 426	04 55 36.96	+30 17 55.3	10.85	1.02	0.10	+0.5	0.00	K0	3.72	+0.23	1
HBC 79	04 55 59.38	+30 34 01.6	9.15	0.89	0.88	+4.0	0.38	G2	3.77	+1.11	1
HBC 427	04 56 02.02	+30 21 03.8	11.60	1.28	0.20	+0.7	0.00	K7	3.61	−0.09	1
HBC 429	05 03 06.60	+25 23 19.7	13.12	1.51	0.42	+9.0	0.25	K7	3.61	−0.29	1
ScoPMS 21	16 01 25.64	−22 40 40.3	11.45	1.10	0.11	−0.35	0.07	K1	3.71	+0.00	4
HBC 630	16 11 08.91	−19 04 46.9	11.90	1.32	0.14	−0.71	0.63	K2	3.69	+0.32	4, 5
HBC 633	16 11 59.28	−19 06 53.3	11.65	1.09	0.16	+0.27	0.49	K1	3.71	+0.04	4, 5
HBC 636	16 25 49.64	−24 51 31.9	13.12	1.7	0.4	−1.3	0.21	K6	3.60	−0.20	3, 4, 5, 6
HBC 637	16 26 03.02	−24 23 36.0	13.95	0.83	0.28	−0.60	2.17	K0	3.72	+1.18	3, 4, 7, 8

NOTE.—Units of right ascension are hours, minutes, and seconds, and units of declination are degrees, arcminutes, and arcseconds.

REFERENCES.—(1) Kenyon & Hartmann 1995; (2) Jones & Herbig 1979; (3) Simon et al. 1995; (4) Walter et al. 1994; (5) Chen et al. 1995; (6) Nürnberger et al. 1998; (7) Bouvier & Appenzeller 1992; (8) Bontemps et al. 2001.

star-forming regions is their rather large distance, about 150 pc. Even with the superb resolution available with the PC2 on *HST*, we are limited to projected separations larger than about 30 AU.

After solar-type stars emerge from the clouds of gas and dust that enshrouded their birth, they collapse rapidly toward the main sequence on timescales of a few million years. During this classical T Tauri star (CTTS) stage, there are several manifestations of their youth, such as strong Hα emission and excess infrared emission from a circumstellar disk. This is the critical phase when planets may have the opportunity to form. However, it would be difficult to detect substellar objects directly, because of obscuration by the disk and its competing emission. For the targets of our search we have chosen WTTSs. We presume that these pre–main-sequence stars have recently cleared their circumstellar disks, as evidenced by their weak Hα emission and weak infrared excess, perhaps by the process of forming planets.

In *HST* Cycle 4 we obtained deep images of nine WTTSs in Taurus-Auriga with the PC2 F785LP filter centered near 870 nm but found no evidence for substellar companions (Sartoretti et al. 1998). For our Cycle 6 proposal we shifted to the longest passband available with the PC2, the W1042 filter, because estimates based on newly available theoretical and observed spectra for brown dwarfs (Oppenheimer et al. 1998; Sudarsky et al. 2003) suggested that the detection limit would be better in this filter despite the low sensitivity of the PC2 CCDs longward of 1000 nm. Deep images of 15 WTTSs were obtained in Cycle 6, but once again no evidence was found for substellar companions down to a detection limit of a few $M_{\rm J}$.

2. TARGET SELECTION AND CHARACTERISTICS

2.1. *Weak-Lined T Tauri Stars*

As targets for this project we focused on WTTSs, pre–main-sequence stars with much weaker emission from their circumstellar disks than CTTSs, presumably because the disks around the WTTSs have recently been dissipated, perhaps by the formation of planets. We tried to select especially young WTTSs in the Taurus-Auriga and Ophiuchus star-forming regions, in order to minimize the cooling time and thus maximize the thermal emission from any substellar companions. Specifically, we selected the youngest stars that met the requirement that the equivalent width of the Hα emission be less than 10 Å or that the $K-L$ color index, when available, be less than 0.4 mag. We also tried to avoid WTTSs with stellar companions that might have interfered with the formation and/or survival of the substellar companions we were looking for. Specifically, we required that our targets had been searched for nearby stars (where "nearby" only means "with small angular separations") using CCD imaging, speckle imaging, and/or lunar occultations and had not been found to have any nearby stars in the range of projected separations, $0\farcs1$–$10''$ (Leinert et al. 1993; Ghez et al. 1993; Simon et al. 1995; Reipurth & Zinnecker 1993; Richichi et al. 1994).

The characteristics of the 17 stars that ended up getting observed in Cycle 6 are summarized in Table 1. Our original selection of WTTSs was based primarily on the Hα equivalent widths reported by Strom et al. (1989), but Table 1 lists more recent values of the Hα equivalent widths and $K-L$ colors, mostly from Kenyon & Hartmann (1995). In three cases (HBC 79, 419, and 429) the new data indicate that these three stars violate our original selection criteria by modest amounts.

The positions that we report for our targets in Table 1 were taken from the 2MASS catalog. The effective temperatures, $T_{\rm eff}$, were all derived from published spectral types using the calibration from Kenyon & Hartmann (1995). The values for the extinction in the Z band, A_Z, were derived from published J-band extinction estimates when available and from V-band estimates otherwise, using the mean extinction curve reported by Fitzpatrick (1999). The luminosities were taken from the literature, mostly from Kenyon & Hartmann (1995). Figure 1 shows our 15 targets on a luminosity versus $T_{\rm eff}$ diagram together with the evolutionary tracks for pre–main-sequence stars from Seiss et al. (2000, hereafter SDF00).

HBC 400 is a double-lined spectroscopic binary. Our TODCOR analysis (see § 2.2.2) of our observed spectra of HBC 400 yielded a light ratio between the secondary and primary of 0.75 at an

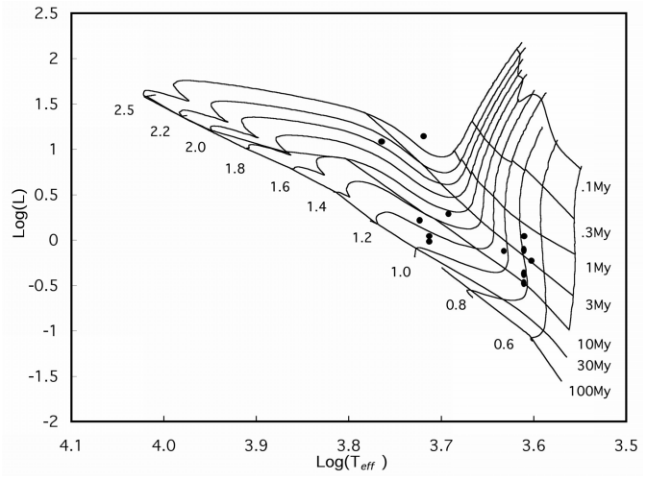

FIG. 1.—Luminosity vs. effective temperature for our 15 targets, with the theoretical evolutionary tracks from SDF00.

TABLE 2
$T_{\rm eff}$ AND log g COMPARISON

	CfA		Literature		CfA−Lit	
Star	$T_{\rm eff}$	log g	$T_{\rm eff}$	log g	$T_{\rm eff}$	log g
HBC 374	4497	3.5	4074	3.4	+423	+0.1
HBC 376	4676	4.0	4074	4.1	+602	−0.1
HBC 397	4505	3.5	4074	4.0	+431	−0.5
HBC 399	4502	4.0	4074	3.7	+428	+0.3
HD 283759	6322	3.5	6456	4.1	−134	−0.6
HBC 419	4581	4.0	4365	4.0	+216	0.0
HBC 426	5026	4.0	5248	4.1	−222	−0.1
HBC 79	5523	3.5	5888	3.6	−365	−0.1
HBC 427	4490	3.5	4074	3.7	+416	−0.2
HBC 429	4553	4.0	4074	4.0	+479	0.0
ScoPMS 21	4801	4.0	5129	4.2	−328	−0.2
HBC 630	4997	4.0	4897	4.0	+100	0.0
HBC 633	4958	3.5	5129	4.2	−171	−0.7
HBC 636	4291	3.5	3981		+310	
HBC 637	4874	3.5	5248	3.9	−374	−0.4

effective wavelength of 5187 Å. We used this light ratio to divide the total observed luminosity between the two components.

2.2. *CfA Spectroscopy*

2.2.1. *Radial Velocities*

Perhaps the most fundamental test of whether a star belongs to a young cluster or star-forming region is to compare its distance and space motion with other cluster members. Foreground and background stars that happen to lie in the same direction as the cluster or region should have discrepant distances, while interlopers that happen to be passing through the cluster or region should have discrepant space motions. Historically, the identification of candidate members of young clusters and star-forming regions has had to rely heavily on observed indicators of youth, because reliable measurements of the individual stellar distances and kinematics have rarely been available. In particular, surveys for stars with strong Hα emission have been a main tool for finding CTTSs, while other indicators such as strong X-ray emission have been used for the identification of WTTSs (Strom et al. 1989).

To provide additional information for checking the membership of our Cycle 6 targets in their respective star-forming regions, we undertook a program of spectroscopic observations with the CfA Digital Speedometers (Latham 1985, 1992), primarily to derive radial velocities. A single radial velocity measurement cannot provide conclusive confirmation or rejection of a star's membership in a star-forming region, because the observed velocity can be perturbed significantly by orbital motion if the target is actually a spectroscopic binary. Therefore, we monitored the velocities of all our targets for several years to allow the identification of spectroscopic binaries and the determination of orbital solutions and systemic velocities when appropriate.

Three nearly identical echelle spectrographs have been used on the MMT and 1.5 m Tillinghast Reflector at the F. L. Whipple Observatory atop Mount Hopkins, Arizona, and on the 1.5 m Wyeth Reflector located at the Oak Ridge Observatory in the town of Harvard, Massachusetts. Photon-counting intensified Reticon detectors were used to record about 45 Å of spectrum in a single order. Most of the spectra were centered near 5187 Å, but a significant number of the early spectra were centered near 5197 Å. The spectral resolution is about 8.5 km s^{-1} for all our exposures, and the signal-to-noise ratios range from about 5 to 50 per resolution element.

Radial velocities were extracted from the observed spectra using the one-dimensional correlation package R2RVSAO (Kurtz & Mink 1998) running inside the IRAF[4] environment. For the templates we used a new grid of synthetic spectra (J. A. Morse & R. L. Kurucz 2005, in preparation) calculated using the latest Kurucz model atmospheres. The new grid of synthetic templates incorporates several improvements compared with the older grid that we used for several years (Nordström et al. 1994).To select the optimum synthetic template for each star, we adopted solar metallicity and ran correlations for an appropriate range of $T_{\rm eff}$; surface gravity, log g; and rotational velocity, $v_{\rm rot}$. For the final velocity reductions we adopted the template that gave the highest average value for the peak of the correlation coefficient.

We also used our grid of correlation results to interpolate for the best effective temperature at the best surface gravity for each of our targets. These $T_{\rm eff}$ and log g values, derived from the CfA spectra alone, are compared in Table 2 with the $T_{\rm eff}$ values that we adopted from the literature and to log g values that we calculated using the masses implied by the SDF00 isochrones plotted in Figure 1. The two sets of temperatures have a mean difference of $+121 \pm 350$ K rms, with a clear dependence of the differences on $T_{\rm eff}$. At the lower temperatures the CfA spectroscopic temperatures are hotter, and at the higher temperatures they are lower. The corresponding mean difference in log g is -0.2 ± 0.3.

Although it is reassuring that our procedure for selecting optimum templates picks stellar parameters that agree reasonably well with values from the literature, we must caution that our procedure was designed to optimize the radial velocity determinations, not to determine the fundamental astrophysical characteristics of our stars. In particular, if the actual metallicity of a star is significantly different from solar, the $T_{\rm eff}$ and log g values that give the best correlations will exhibit systematic errors. For example, if the star is actually more metal-poor than the Sun, then the observed absorption lines will be weaker than in a synthetic template spectrum with the correct temperature and gravity

[4] IRAF (Image Reduction and Analysis Facility) is distributed by the National Optical Astronomy Observatory, which is operated by the Association of Universities for Research in Astronomy, Inc., under contract with the NSF.

TABLE 3
MEAN VELOCITIES AND ERRORS

Star	$T_{\rm eff}$	log g	$N_{\rm obs}$	Span	$v_{\rm rot}$	$v_{\rm rad}$	σ	ext	int	e/i	χ^2	$P(\chi^2)$	Binary
HBC 374	4500	3.5	21	6675	17	+15.93	0.39	1.81	0.97	1.86	87.27	0.000000	
HBC 376	4750	4.0	7	1475	70	+16.06	1.27	3.35	3.04	1.10	9.38	0.153129	
HBC 397	4500	3.5	29	5470	35	+17.63	0.32	1.72	1.26	1.37	51.15	0.004802	
HBC 399	4500	4.0	20	4776	21	+14.62	0.47	2.10	1.40	1.50	43.68	0.001045	
HBC 400	4500	4.0	17	4082	4	+17.63	0.18						SB2
HD 283759	6250	3.5	6	1433	56	+31.63	0.86	1.64	2.11	0.78	5.32	0.377924	
HBC 419	4500	4.0	9	4041	15	+16.02	0.49	1.46	0.98	1.48	24.87	0.001634	
HBC 426	5000	4.0	22	4752	23	+14.08	0.21	0.95	0.99	0.96	20.42	0.494821	
HBC 79	5500	3.5	21	7740	65	+14.71	0.40	1.84	1.81	1.02	26.66	0.145004	
HBC 427	4500	3.5	58	5148	11	+14.42	0.11	5.48	0.65	8.39	4323.92	0.000000	SB1
HBC 429	4500	4.0	19	3719	12	+17.56	0.40	1.76	0.91	1.94	66.74	0.000000	
ScoPMS 21	5000	4.0	11	4402	11	−6.34	0.26	0.86	0.69	1.25	15.58	0.112360	
HBC 630	5000	4.0	31	1181	25	−6.55	0.37	9.89	1.19	8.30	2805.03	0.000000	SB1
HBC 633	5000	3.5	18	824	26	−7.36	0.40	9.07	1.00	9.10	1615.39	0.000000	SB1
HBC 636	4250	3.5	13	5409	6	−5.29	0.19	0.64	0.68	0.94	11.02	0.526802	
HBC 637	5000	3.5	5	356	29	−4.62	3.32	7.43	4.31	1.73	21.70	0.000229	

but solar metallicity. To regain the best match with the observed spectrum, a template with weaker lines is needed, i.e., with hotter temperature and/or weaker surface gravity than the correct values. In contrast, the values that we derive for the projected rotational velocity, $v_{\rm rot}\sin i$, are relatively insensitive to errors in the other template parameters, except when the rotation is smaller than about 5 km s^{-1}; i.e., it is much smaller than the instrumental resolution of 8.5 km s^{-1}.

2.2.2. *Spectroscopic Binaries*

The results of our radial velocity observations are summarized in Table 3, where we report the $T_{\rm eff}$ and log g values adopted for the template spectra; the number of observations and time spanned in days; the projected rotational velocity, $v_{\rm rot}\sin i$; the mean radial velocity and error in the mean (or the systemic velocity and its error for the four spectroscopic binaries with orbital solutions); the observed rms velocity variation (ext), mean internal velocity error estimate (int), and ratio of ext to int (e/i); and the χ^2 value and probability calculated assuming a floor error of 0.25 km s^{-1}. Four of our targets are spectroscopic binaries according to the criteria described by Latham et al. (2002); one of them is double-lined. These stars are noted in the final column of Table 3. The details of the orbital solutions are documented in Table 4, and the velocity curves are plotted in Figure 2. The individual velocities are listed in Table 5, including velocities for both components of the double-lined binary HBC 400 derived using the two-dimensional correlation technique TODCOR (Zucker & Mazeh 1994) as implemented by G. T. at CfA. For a more complete description of the procedures used for the radial velocity determinations and orbital solutions, see Latham et al. (2002).

2.2.3. *Radial Velocity Membership*

Ten of our Cycle 6 targets in the Taurus-Auriga region have radial velocities in the range +14.08–17.63 km s^{-1}, with an average velocity of $+15.89 \pm 0.41$ km s^{-1} and an rms dispersion of 1.30 km s^{-1}. Our eleventh Taurus-Auriga target, HD 283759, has a velocity of $+31.63 \pm 0.86$ km s^{-1}, which is larger than the cluster mean by 12 times the dispersion. We conclude that HD 283759 cannot be a member of the Taurus-Auriga star-forming region. Although its $K - L = 0.00$ mag suggests that it may be young, it does not have a direct distance determination and therefore cannot be placed on an H-R diagram to estimate its age. We cannot assume that it has the same distance as Taurus-Auriga and was born in that star-forming region a few million years ago, because its higher radial velocity would have moved it further away by 78 pc in 5 Myr. The velocity dispersion of 1.30 km s^{-1} that we find for our 10 confirmed members is consistent with the dispersion of 1–2 km s^{-1} reported by Jones & Herbig (1979) for subgroups in Taurus-Auriga, based on

TABLE 4
ORBITAL SOLUTIONS

HBC	P	γ	K	e	ω	T	$a_1\sin i$ $a_{1,2}\sin i$	$f(M)$ $M_{1,2}\sin^3 i$	N σ	Span Cycles
400a	3.887763	+17.63	18.42	0.025	57	47886.42	0.984	0.01013	17	4082
	±0.000039	±0.18	±0.32	±0.016	±30	±0.33	±0.019	±0.00057	0.90	1050
400b			18.49				0.988	0.01009	17	
			±0.43				±0.026	±0.00048	1.22	
427	2533	+14.42	7.54	0.469	214.4	49120	232.3	0.0778	58	5149
	±13	±0.11	±0.18	±0.019	±2.9	±15	±7.1	±0.0070	0.77	2.0
630	144.73	−6.55	15.01	0.253	258.7	47047.6	28.9	0.046	31	1181
	±0.42	±0.37	±0.61	±0.044	±7.6	±2.7	±3.7	±0.017	1.74	8.2
633	10.4012	−7.36	14.94	0.179	300	51427.30	2.10	0.0034	18	825
	±0.0014	±0.40	±0.59	±0.042	±10	±0.27	±0.23	±0.0011	1.39	79.3

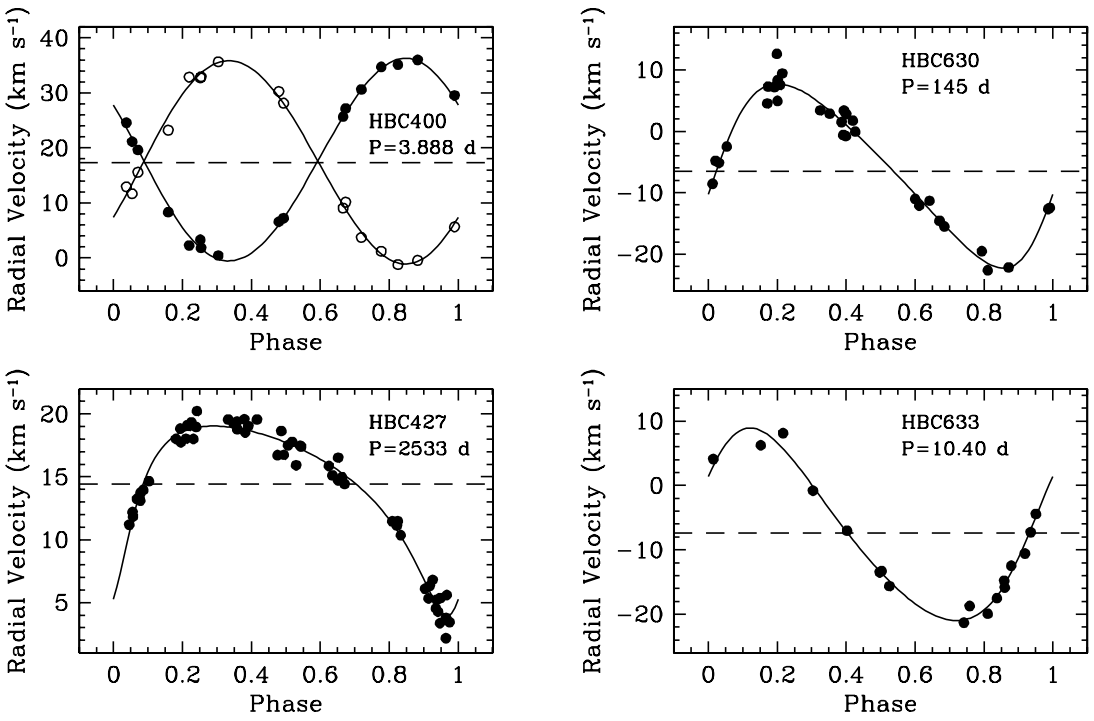

FIG. 2.—Velocity curves for our orbital solutions of four spectroscopic binaries, together with the observed radial velocities.

proper-motion measurements. When we combine the velocities for the 10 members confirmed in this paper with all the CfA velocities now available for the eight members confirmed in our Cycle 4 paper (Sartoretti et al. 1998), we get an average velocity of $+16.28 \pm 0.30$ km s^{-1} and an rms dispersion of 1.26 km s^{-1}. As summarized in Table 6, our results are reasonably consistent with the mean velocities and rms dispersions for the Taurus-Auriga star-forming region as reported by Hartmann et al. (1986) for 41 CTTSs, by Hartmann et al. (1987) for eight Lick Ca II CTTSs showing strong lithium, and by Walter et al. (1988) for 29 WTTSs.

All five of our targets in Ophiuchus have similar velocities, with a mean of -6.0 ± 0.5 km s^{-1} and a dispersion of 1.1 km s^{-1}. This is consistent with the mean velocity of -5.2 km s^{-1} and a dispersion of 1.8 km s^{-1} reported by Walter et al. (1994) for a larger sample of young stars in Ophiuchus.

3. *HST* OBSERVATIONS AND DATA REDUCTION

For our *HST* observations with the PC2 we chose the near-infrared intermediate-band filter W1042 (Z band). The transmission of this filter is nearly flat for $\lambda = 1045 \pm 45$ nm with a steep decline outside this range, but the integrated response of the system is narrower and shifted to a shorter effective wavelength because of the exponential decline in sensitivity of the CCD at wavelengths longer than about 1000 nm. Accordingly, the effective passband of the PC2 in the W1042 filter is nominally $\lambda = 1025 \pm 25$ nm. The PC2 has a pixel spacing of 0.″0455, and the point-spread function (PSF) has a FWHM in the W1042 filter of 0.″11.

For each of the stars we obtained images at two spacecraft roll angles 25° apart to allow us to distinguish between PSF artifacts (which would appear at the same position for both roll angles) and the signature of a nearby object (which would appear to rotate by 25° between the two roll angles). Unfortunately, we did not require that the two roll angles be obtained on successive orbits. In actual execution of this project, the two roll angles were always separated by at least a day, with a median interval between roll angles of 32 days and a maximum of 279 days. It turns out that there is significant "breathing" in the *HST* optics even over 1 day, resulting in subtle changes in the PSF that limit how well the subtraction of the two roll angles removes PSF artifacts. Obtaining the two roll angles in successive orbits would also have helped minimize the impact of intrinsic brightness variations in our targets.

Four separate images were obtained during a single orbit at each roll angle. An exposure time of 400 s was chosen for the individual exposures, so as to mildly saturate the centers of the target star images. The four exposures were taken in pairs, with an offset of 5 pixels in both x and y between the pairs, to allow better identification of warm pixels suffering from imperfect correction.

After processing through the standard *HST* pipeline, the images were reduced with standard IRAF tasks. This included preliminary processing with *warmpix* to correct for flawed pixels, using the appropriate monthly map; registration of the two pairs of offset images using *xreg*; removal of cosmic rays using *crrej*; and subtraction of the summed images at the two roll angles using *imarith*.

3.1. *Photometry of the Targets*

We used the IRAF aperture photometry task *phot* to determine the instrumental Z magnitudes, using the standard aperture with radius 0.″5 for the star and an annulus between 150 and 155 pixels from the center of the target for the background. An aperture correction of -0.1 mag was then applied to account for the target flux in the PSF wings outside the 0.″5 aperture.

HBC 633/1 is a relatively bright but unsaturated object close to HBC 633, 2.13 mag fainter in the Z band and at a separation of 3.″41. To correct for the saturation at the center of the target images, we used the image of HBC 633/1 to calibrate the signal expected inside an aperture with radius 7 pixels compared with the signal in an annulus between 7 and 10.8 pixels. This ratio

TABLE 5
RADIAL VELOCITIES

Telescope[a]	HJD	v_{rad}	σ
HBC 374, 04 18 46.9 +28 20 09			
T	2445630.9144	16.73	0.72
M	2446036.6871	13.31	0.72
T	2446364.8450	17.77	0.88
T	2446372.9005	15.59	1.12
T	2446372.9228	16.22	1.24
T	2446373.8358	14.67	0.87
T	2446373.8579	14.42	0.78
M	2446389.7204	14.29	0.89
M	2446745.7226	16.84	0.89
T	2446776.6847	17.11	0.96
T	2447073.8547	17.04	0.91
T	2447075.8694	17.52	1.03
M	2447127.6702	18.56	0.67
T	2447437.9696	17.37	0.99
T	2447459.8820	17.52	0.85
M	2447493.8078	16.56	1.11
M	2450800.8925	17.69	1.23
T	2451857.9903	12.89	0.77
T	2451892.9003	11.85	0.87
T	2452238.8859	15.32	0.88
T	2452306.7482	15.00	0.96
HBC 376, 04 18 51.7 +17 23 17			
M	2450800.8820	14.38	1.88
M	2450826.7749	17.64	2.39
T	2451448.8790	19.30	3.87
T	2451564.7135	19.16	4.40
T	2451857.9758	15.14	3.38
T	2452238.9157	9.71	2.41
T	2452276.7049	17.02	2.84
HBC 397, 04 32 09.3 +17 57 23			
T	2446422.6583	12.78	1.78
T	2446429.7171	15.64	1.36
M	2446448.8185	20.60	0.89
T	2446727.9328	17.45	1.37
M	2447075.8032	18.66	0.96
T	2447162.8001	13.74	1.24
T	2447200.6697	18.50	1.02
M	2447492.8333	17.85	1.31
T	2447513.7117	17.35	0.80
T	2447518.7390	15.32	1.26
T	2447519.7218	18.24	1.50
T	2447543.6686	18.64	1.19
T	2447544.6101	17.99	0.98
M	2447546.5925	17.35	0.76
T	2447555.6624	18.65	1.17
T	2447578.6982	17.14	0.72
T	2447790.9996	16.96	1.69
T	2447791.9048	17.51	1.99
T	2447791.9158	18.62	1.27
T	2447810.9601	17.43	1.18
T	2447822.8268	17.68	1.22
T	2447837.7570	19.73	0.96
T	2447840.7576	17.50	1.00
T	2447868.9142	19.28	1.26
M	2448201.8573	18.05	1.18
T	2450771.7253	18.25	1.12
M	2450800.9133	20.32	1.15
T	2451856.8612	18.21	1.73
T	2451892.9256	15.56	1.36

TABLE 5—*Continued*

Telescope[a]	HJD	v_{rad}	σ
HBC 399, 04 32 14.6 +18 20 15			
T	2447080.9051	16.99	1.26
T	2447494.7465	10.12	1.62
T	2447523.6435	15.01	1.25
T	2447543.6380	12.64	0.98
M	2447546.5740	13.25	1.20
T	2447555.6444	15.33	1.18
T	2447578.7183	12.93	1.16
T	2447791.0132	13.57	1.48
T	2447791.9270	12.40	1.73
T	2447810.9103	15.09	1.78
T	2447815.9393	15.03	0.93
T	2447822.0319	13.59	1.53
T	2447822.8015	13.80	1.18
T	2447837.7952	18.76	1.75
M	2447896.5783	14.07	0.92
T	2447903.6639	13.25	1.87
T	2449707.7556	14.56	1.23
T	2450771.7387	16.94	1.03
M	2450800.9211	18.05	1.07
T	2451856.8756	16.67	1.77
HBC 400, 04 32 15.8 +18 01 39			
T	2446689.974	1.83	
		32.91	
T	2447815.982	36.00	
		−0.42	
T	2447819.029	25.71	
		9.05	
T	2447837.742	6.59	
		30.28	
T	2447840.745	3.35	
		32.75	
T	2447842.785	34.73	
		1.20	
T	2447843.864	21.15	
		11.66	
T	2447844.835	0.45	
		35.66	
T	2447846.862	35.17	
		−1.20	
T	2447847.816	19.63	
		15.59	
T	2447868.898	7.23	
		28.13	
T	2447869.776	30.61	
		3.70	
T	2447870.827	29.53	
		5.67	
T	2447871.720	2.27	
		32.89	
T	2447878.787	24.59	
		12.93	
T	2447900.700	27.17	
		10.16	
T	2450771.755	8.32	
		23.23	
HD 283759, 04 36 49.1 +24 12 59			
W	2450804.6480	30.33	3.91
M	2450826.8184	28.80	1.71
W	2450846.5512	32.54	2.31
T	2451622.6105	31.13	1.26
T	2451856.8481	33.99	1.61
T	2452237.7810	32.25	1.60

TABLE 5—*Continued*

Telescope[a]	HJD	v_{rad}	σ
HBC 419, 04 39 17.8 +22 21 04			
T	2447523.6647	14.50	1.61
T	2447838.7962	14.89	0.77
M	2447897.7448	18.17	0.77
M	2447901.5863	16.51	0.75
T	2449707.7419	13.85	0.80
T	2450771.7864	15.87	0.89
M	2450799.9421	15.47	1.70
M	2450826.8252	17.65	0.60
T	2451564.7285	17.21	0.90
HBC 426, 04 55 37.0 +30 17 55			
T	2447524.6653	13.91	0.78
T	2447838.8058	16.16	0.69
M	2447897.5990	14.23	1.09
M	2447899.5793	15.34	0.85
T	2448169.9607	14.13	0.88
T	2448194.9725	14.30	0.65
M	2448910.8106	13.07	0.91
T	2448940.9245	12.44	1.05
T	2448968.8477	13.52	1.02
T	2448988.7914	15.98	1.21
T	2449058.6019	14.03	1.27
T	2449707.8448	14.21	1.21
W	2450771.7518	15.01	1.27
M	2450826.8310	14.24	0.95
W	2450846.5240	13.85	0.85
W	2450889.6084	12.71	1.08
W	2451102.8114	13.85	0.86
W	2451186.6841	14.74	1.01
T	2451622.6240	13.23	0.77
T	2451856.8399	13.61	1.03
T	2452240.8069	14.17	0.93
W	2452276.6343	13.34	1.09
HBC 79, 04 55 59.3 +30 34 02			
T	2444916.9578	14.62	2.40
T	2444916.9920	14.37	2.20
T	2444917.0205	13.17	2.30
T	2444918.0203	14.80	1.16
T	2444919.0329	16.34	1.73
T	2444920.0273	12.69	3.50
T	2445630.0332	17.00	1.13
M	2445709.7597	16.08	0.88
T	2445719.7802	15.40	1.60
T	2445983.9992	11.50	1.09
T	2445987.0179	15.61	2.21
T	2446013.0338	15.21	0.67
M	2446037.9347	13.79	2.26
M	2446724.0267	13.72	1.34
M	2446745.9908	17.23	1.94
W	2450771.7639	15.30	1.71
W	2450804.7085	18.27	1.54
M	2450826.8354	15.59	1.08
W	2450846.5089	15.11	1.37
W	2451856.7868	12.57	2.92
W	2452657.7439	11.69	2.55

TABLE 5—*Continued*

Telescope[a]	HJD	v_{rad}	σ
HBC 427, 04 56 02.2 +30 21 04			
T	2446421.7465	4.56	0.48
T	2446428.6908	5.20	0.59
T	2446451.6493	3.36	0.46
T	2446728.8723	11.83	0.74
T	2446775.7779	13.25	0.58
T	2446804.6601	13.96	0.62
T	2447045.0072	18.02	0.58
M	2447075.8235	18.83	0.48
T	2447080.8802	17.74	0.64
T	2447127.8693	19.09	0.56
T	2447138.7851	19.04	0.50
M	2447157.5923	19.33	0.57
T	2447192.6570	18.96	0.60
T	2447198.6334	20.23	0.70
T	2447427.9813	19.56	0.82
M	2447492.8084	19.40	0.61
M	2447546.5819	19.57	0.57
T	2447576.6672	19.04	0.74
T	2447791.0070	16.72	0.63
T	2447818.8031	18.64	0.95
T	2447837.7737	16.75	0.49
T	2447868.9265	17.50	0.56
M	2447899.5658	17.75	0.44
M	2447928.6599	15.91	0.48
T	2447957.6174	17.46	0.50
T	2447965.6088	17.40	0.51
T	2448168.9077	15.87	0.56
T	2448194.9668	15.12	0.50
T	2448284.7374	14.42	0.57
T	2448635.7208	11.46	0.43
M	2448669.5846	11.11	0.44
T	2448675.6737	11.47	0.49
T	2448697.6310	10.35	0.59
T	2448875.9712	6.10	0.56
T	2448901.9111	5.32	0.55
M	2448910.8050	6.33	0.52
T	2448931.9191	6.80	0.50
T	2448970.8279	4.28	0.63
T	2448988.7715	5.36	0.52
T	2449030.7092	3.79	0.56
T	2449056.6039	3.44	0.51
M	2449235.0189	11.18	0.48
T	2449258.9979	12.19	0.47
T	2449290.8841	13.24	0.42
T	2449316.8181	13.11	0.58
T	2449318.8321	13.72	0.58
T	2449379.6723	14.64	0.66
T	2449652.0325	18.02	0.48
T	2449706.8549	18.02	0.55
T	2450000.9524	19.24	0.49
T	2450029.9190	18.76	0.54
T	2450087.7501	18.52	0.48
W	2450173.5381	19.54	0.93
W	2450771.7773	16.52	0.64
T	2450771.7981	14.70	0.42
M	2450799.9570	14.97	0.61
W	2451563.5879	2.17	1.25
W	2451570.4936	5.60	0.74

TABLE 5—*Continued*

Telescope[a]	HJD	v_{rad}	σ
HBC 429, 05 03 06.6 +25 23 20			
T	2447080.9202	19.90	1.23
T	2447494.7730	14.04	0.76
T	2447523.6782	19.11	0.98
T	2447543.6474	15.75	0.78
T	2447555.7002	17.06	0.82
T	2447791.9351	14.89	0.86
T	2447810.9199	16.74	0.86
T	2447816.8702	19.78	0.95
T	2447822.8656	17.62	0.56
T	2447837.7836	18.55	0.86
T	2447841.8150	17.23	1.03
M	2447844.7475	17.31	0.72
M	2447896.5891	18.51	0.93
T	2449354.7092	17.94	0.75
T	2449355.6827	18.11	0.86
T	2449412.6686	21.17	1.01
T	2449706.8396	15.84	0.64
T	2450771.8211	17.43	1.02
M	2450799.9063	16.78	0.75
ScoPMS 21, 16 01 25.6 −22 40 40			
M	2446565.7987	−6.10	0.58
T	2446872.9759	−5.35	0.57
T	2447280.8999	−6.32	0.67
M	2447546.0640	−6.57	0.57
M	2447668.7598	−5.34	0.65
T	2448017.9006	−6.98	0.53
M	2448783.7622	−6.66	0.69
M	2448873.6153	−7.62	0.69
T	2450884.9736	−5.14	0.77
T	2450914.9773	−7.64	0.60
T	2450967.7585	−5.98	0.68
HBC 630, 16 11 08.9 −19 04 46			
M	2446450.0523	−22.16	0.58
M	2446565.7460	−14.56	0.91
M	2446567.7418	−15.50	1.31
M	2446815.0395	3.37	0.85
T	2446872.9608	−19.53	1.59
T	2446927.9406	7.29	1.12
T	2446931.9244	8.29	0.87
T	2446932.9444	7.53	0.93
T	2446933.8887	9.40	0.99
T	2446949.8280	3.39	1.69
M	2446953.8195	2.85	0.86
M	2446958.8022	1.49	0.98
M	2446960.7231	2.78	1.26
M	2446989.7004	−10.99	1.43
T	2446995.7235	−11.30	1.72
T	2447045.6136	−12.63	1.14
T	2447050.6094	−4.83	1.71
M	2447076.5912	4.94	1.29
M	2447217.0360	4.52	1.38
T	2447220.0437	7.16	1.36
T	2447221.0493	12.62	1.21
M	2447248.9587	−0.62	0.90
T	2447249.9939	−0.80	1.12
T	2447252.9947	1.73	1.10
T	2447253.9972	−0.05	1.16
T	2447280.8632	−12.08	1.43
M	2447309.6594	−22.61	1.05
T	2447335.7705	−12.44	1.03
T	2447338.7911	−8.54	0.97
T	2447344.7444	−2.47	1.03
T	2447630.9424	−5.15	1.08

TABLE 5—*Continued*

Telescope[a]	HJD	v_{rad}	σ
HBC 633, 16 11 59.2 −19 06 52			
T	2450884.9643	−14.80	1.56
T	2450914.9535	−21.32	0.92
T	2450968.8033	−10.57	0.88
T	2450969.7958	4.10	1.09
T	2450972.8032	−0.80	1.27
T	2451352.7995	−17.50	0.76
T	2451359.7239	−13.27	1.71
T	2451593.0506	−7.25	1.08
T	2451619.9856	−15.64	0.77
T	2451622.9551	−19.92	0.80
T	2451647.9826	8.11	0.80
T	2451649.9118	−7.04	0.74
T	2451650.8971	−13.49	0.68
T	2451654.8687	−12.45	0.54
T	2451684.8177	−18.72	0.81
T	2451685.8747	−15.86	0.77
T	2451686.8167	−4.43	1.02
T	2451709.7153	6.25	0.97
HBC 636, 16 25 49.7 −24 51 31			
M	2446955.8539	−5.03	0.58
M	2447309.8224	−5.47	0.50
M	2447669.8123	−4.34	0.50
M	2448046.7901	−4.77	0.42
T	2448402.9038	−4.18	0.63
M	2448784.7692	−5.07	0.40
T	2450967.7744	−5.21	0.66
T	2451354.7430	−6.45	0.65
T	2451650.9345	−5.66	0.69
T	2451685.8282	−5.42	0.65
T	2452072.8065	−5.21	0.69
T	2452364.9591	−5.86	0.77
T	2452365.0137	−5.99	1.02
HBC 637, 16 26 03.1 −24 23 36			
T	2451353.7793	−14.84	2.22
T	2451360.6986	−0.49	7.28
T	2451685.8518	1.13	2.16
T	2451686.8346	6.43	3.64
T	2451709.8073	−7.60	1.98

NOTE.—Units of right ascension are hours, minutes, and seconds, and units of declination are degrees, arcminutes, and arcseconds. Table 5 is also available in machine-readable form in the electronic edition of the *Astronomical Journal*.

[a] T = Tillinghast Reflector, M = MMT, W = Wyeth Reflector.

TABLE 6

MEAN VELOCITIES FOR OUR STAR-FORMING REGIONS

Sample	$\langle v_{rad} \rangle \pm \sigma$ (km s^{-1})	rms (km s^{-1})	N_{stars}	Reference
Tau-Aur Cycle 6	+15.89 ± 0.41	1.30	10	1
Tau-Aur Cycles 6 & 4	+16.28 ± 0.30	1.26	18	1
Tau-Aur CTTSs	+17.40 ± 0.33	2.13	41	2
Tau-Aur LkCa CTTSs	+15.70 ± 0.33	0.94	8	3
Tau-Aur WTTSs	+16.23 ± 0.53	2.85	29	4
Oph Cycle 6	−6.03 ± 0.48	1.08	5	1

REFERENCES.—(1) This paper; (2) Hartmann et al. (1986); (3) Hartmann et al. (1987); (4) Walter et al. (1988).

TABLE 7
JOURNAL OF *Hubble Space Telescope* OBSERVATIONS

Star	Alias	JD	Z	ΔZ_{corr}	J	H	K
HBC 374	V1023 Tau	2451189.61	9.15	−0.37	8.52	7.60	7.28
		2451257.26	9.11	−0.38			
HBC 376	V1069 Tau	2451170.21	10.30	−0.13	9.94	9.33	9.19
		2451171.13	10.23	−0.15			
HBC 397	V1075 Tau	2450773.14	9.94	−0.20	9.72	9.04	8.85
		2450776.23	9.81	−0.24			
HBC 419	V1079 Tau	2450786.25	9.71	−0.30	9.43	8.59	8.18
		2450813.87	9.64	−0.31			
HBC 426	V396 Aur	2451112.36	9.06	−0.41	8.86	8.31	8.18
		2451113.36	9.10	−0.41			
HBC 427	V397 Aur	2451558.22	9.30	−0.37	8.95	8.29	8.13
		2451279.65	9.25	−0.38			
HBC 400	V826 Tau	2451179.14	9.49	−0.33	9.16	8.47	8.25
		2451206.75	9.46	−0.33			
HBC 399	V827 Tau	2451175.25	9.83	−0.24	9.11	8.43	8.14
		2451206.82	9.51	−0.30			
HBC 429	V836 Tau	2450761.23	10.37	−0.11	9.84	9.05	8.75
		2450765.28	10.12	−0.18			
HBC 79	SU Aur	2451175.18	7.22	−1.28	7.19	6.53	5.98
		2451280.65	7.17	−1.28			
HD 283759		2450773.28	8.81	−0.45	8.70	8.42	8.32
		2450775.22	8.84	−0.45			
ScoPM S21	V1152 Sco	2450850.40	9.60	−0.30	9.31	8.69	8.49
		2450867.41	9.60	−0.30			
HBC 630	V1000 Sco	2450678.79	9.13	−0.37	8.66	7.92	7.68
		2450716.91	9.15	−0.37			
HBC 633	V1001 Sco	2450674.76	9.45	−0.29	8.94	8.30	8.08
		2450710.92	9.45	−0.29			
HBC 637	V2246 Oph	2451238.22	9.03	−0.44	8.11	6.87	6.22
		2451251.39	9.05	−0.44			

was then used to estimate the expected signal for the centers of the saturated target images based on the signal measured for them in their 7–10.8 pixel annulus. The saturation corrections ranged from −0.11 mag for V836 Tau to −1.28 mag for SU Aur. The case of SU Aur is also problematic because of the nebulosity around the star.

A journal of the *HST* observations and the fully corrected Z magnitudes for each roll angle are presented in Table 7, together with the saturation correction ΔZ_{corr} and J, H, and K magnitudes from the 2MASS catalog. For the target stars the accuracy of the Z magnitudes is not limited by photon noise but rather by systematic errors, for example, errors in the saturation corrections resulting from telescope breathing and errors in the transformation to a standard Z magnitude system. The scatter in the saturation corrections is on the order of 0.02 mag, and the photon noise in the Z magnitude for HBC 633/1, the star used to calibrate the saturation correction, is on the order of 0.01 mag. Unless there are other systematic errors that contribute significantly, the relative photometry between roll angles should be good to better than 0.03 mag. In a few cases the Z magnitudes for the two different roll angles differ by more than 0.1 mag, presumably because of variations in the intrinsic brightness of these young stars.

3.2. *Photometry and Astrometry of Nearby Objects*

We searched all our subtracted images for evidence of faint nearby objects to our target stars, but none were detected at angular separations of less than 4″, corresponding to a projected separation of 600 AU at the distance to the Taurus-Auriga and Ophiuchus star-forming regions. A total of 19 nearby objects were found at larger separations, as reported in Table 8. Their Z magnitudes were determined with the same procedures as for the targets, except no saturation corrections were needed. The photometric errors quoted in Table 8 include contributions both from photon statistics and from background corrections. We measured the positions of the nearby objects using the IRAF task *xy2rd*. The values of right ascension and declination reported in Table 8 were calculated using the information provided in the image headers and should be accurate to about 0.″5. The separations between the nearby objects and their primaries are much more accurate and should be good to about 0.2 pixels, or 0.″01. Position angles, θ, are measured from north through east.

Seven of our nearby objects have corresponding entries in the 2MASS catalog, five have corresponding entries in the USNO-B1.0 catalog (Monet et al. 2003), and two appear in both catalogs. These matches are reported in Table 9, where the positions and photometry are from the 2MASS and/or USNO-B1.0 catalogs. The positions in the K versus $J - K$ color-magnitude diagram for the three faint nearby objects with somewhat reliable photometry in the 2MASS catalog are plotted in Figure 3 (*squares*), along with all our targets (*triangles*). The solid line shows the main sequence as reported in Cox (2000).

HBC 397/1 is identified in the 2MASS catalog but has unreliable photometry. The J and H magnitudes are flagged as background contaminated, and K is flagged as an upper limit nondetection. Thus, the 2MASS photometry provides little useful information about the nature of this object.

HD 283759/1 is identified in the 2MASS catalog. The 2MASS photometry places HD 283759/1 below the main sequence. It can

TABLE 8
FAINT NEARBY OBJECTS TO THE TARGET STARS

Star	R.A. (J2000)	Decl. (J2000)	Z	σ_Z	ρ (arcsec)	σ_ρ	θ (deg)	σ_θ
HBC 397/1	04 32 09.64	+17 57 26.5	15.93	0.02	7.20	0.01	54.19	0.08
HBC 426/1	04 55 36.61	+30 17 55.4	19.20	0.40	4.31	0.01	279.02	0.13
HBC 426/2	04 55 36.38	+30 18 04.0	14.16	0.01	11.75	0.01	322.50	0.05
HBC 426/3	04 55 35.63	+30 17 50.2	14.58	0.01	17.65	0.01	254.68	0.03
HBC 427/1	04 56 02.73	+30 21 04.0	17.45	0.06	9.12	0.01	91.68	0.06
HD 283759/1	04 36 48.20	+24 12 52.6	12.97	0.01	14.21	0.01	241.17	0.04
HBC 429/1	05 03 07.18	+25 23 16.2	18.50	0.14	8.92	0.01	108.74	0.06
ScoPMS 21/1	16 01 25.85	−22 40 35.6	17.20	0.06	6.16	0.01	37.78	0.09
ScoPMS 21/2	16 01 25.10	−22 40 34.7	18.20	0.18	9.39	0.01	307.94	0.06
ScoPMS 21/3	16 01 25.58	−22 40 38.0	17.34	0.06	9.86	0.01	75.20	0.06
ScoPMS 21/4	16 01 24.58	−22 40 37.5	16.45	0.03	14.50	0.01	282.23	0.04
ScoPMS 21/5	16 01 24.52	−22 40 35.4	17.44	0.06	15.79	0.01	289.10	0.03
ScoPMS 21/6	16 01 24.54	−22 40 32.6	18.07	0.16	16.66	0.01	298.55	0.03
ScoPMS 21/7	16 01 25.78	−22 40 57.9	15.89	0.02	17.56	0.01	170.96	0.03
HBC 630/1	16 11 08.62	−19 04 56.3	19.00	0.30	10.01	0.01	204.17	0.06
HBC 633/1	16 11 59.21	−19 06 55.7	11.58	0.01	3.41	0.01	192.60	0.17
HBC 633/2	16 11 59.06	−19 06 46.0	17.31	0.06	6.91	0.01	335.24	0.08
HBC 633/3	16 11 58.91	−19 07 01.5	18.24	0.10	10.37	0.01	208.28	0.05
HBC 633/4	16 12 00.22	−19 06 48.0	18.43	0.15	14.33	0.01	72.66	0.04

NOTE.—Units of right ascension are hours, minutes, and seconds, and units of declination are degrees, arcminutes, and arcseconds.

easily be explained as a hot background star in the spectral type range F–B and at the corresponding distances ranging from 2 to 5 kpc, assuming the extinction law illustrated by the vector for 7 kpc in Figure 3.

HBC 426/2 is identified in the 2MASS catalog. It also lies below the main sequence, but it is too blue and too faint to be explained as a reddened main-sequence star. The $J - H$ and $H - K$ colors from 2MASS are consistent with this star being a relatively nearby white dwarf (Wachter et al. 2003). All three of the 2MASS magnitudes are flagged as background contaminated, but the quoted errors are small enough to allow this interpretation.

HBC 426/3 is identified in the 2MASS catalog. It also lies below the main sequence but is brighter and redder than HBC 426/2. It could easily be a cool background star. The J magnitude is flagged as background contaminated, but the quoted error is small.

HBC 427/1 is identified in the USNO-B1.0 catalog but does not appear in the 2MASS catalog. For our observed $Z = 17.45$ mag, the Burrows et al. (1997) models predict that a substellar object would have a K magnitude close to the limit of the 2MASS catalog, so the nondetection by 2MASS is not conclusive. The detection at B and R reported by the USNO-B1.0 gives strong evidence that the object is stellar and therefore in the background.

HBC 429/1 is identified in the USNO-B1.0 and is also too faint to appear in the 2MASS catalog. Our Z value is similar to the photographic $R1$ and $R2$ magnitudes listed in the USNO-B1.0, so this is probably a fairly hot star in the background.

ScoPMS 21/4 is identified in the 2MASS catalog. The J and H magnitudes are flagged as background contaminated, and K is flagged as an upper limit nondetection. ScoPMS 21/4 is also identified in the USNO-B1.0 catalog. Our Z value is only half a magnitude brighter than the average of $B1$ and $B2$, so this is

TABLE 9
NEARBY OBJECTS WITH 2MASS AND USNO-B1.0 MATCHES

Star	R.A. (J2000)	Decl. (J2000)	J	H	K	$B1$	$R1$	$B2$	$R2$	Ref.
HBC 397/1	04 32 09.64	+17 57 26.3	15.13	14.72	12.15					1
HD 283759/1	04 36 48.21	+24 12 51.9	12.55	11.99	11.80					1
HBC 426/2	04 55 36.42	+30 18 04.4	13.89	13.51	13.44					1
HBC 426/3	04 55 35.67	+30 17 50.5	14.01	13.41	13.09					1
HBC 427/1	04 56 02.56	+30 21 02.8					19.07	19.55		2
HBC 429/1	05 03 07.11	+25 23 17.8					18.80		17.96	2
ScoPMS 21/4	16 01 24.61	−22 40 36.9	16.14	15.78	14.95					1
	16 01 24.68	−22 40 37.6				17.42	16.15	16.64	15.65	2
ScoPMS 21/5	16 01 24.62	−22 40 35.7						15.25	18.27	2
ScoPMS 21/7	16 01 25.82	−22 40 57.8	15.65	14.88	14.84					1
	16 01 25.80	−22 40 56.9				19.00	17.67	18.46	17.22	2
HBC 633/1	16 11 59.23	−19 06 56.3	9.15	8.47	8.34					1

NOTE.—Units of right ascension are hours, minutes, and seconds, and units of declination are degrees, arcminutes, and arcseconds.
REFERENCES.—(1) 2MASS; (2) USNO-B1.0.

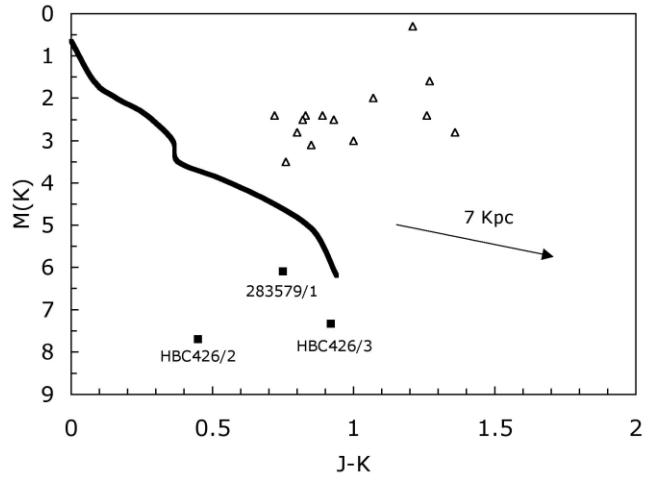

FIG. 3.—The K vs. $J - K$ color-magnitude diagram for our targets (*triangles*) and three faint nearby objects (*squares*). The arrow illustrates the reddening vector expected for stars at a distance of 7 kpc.

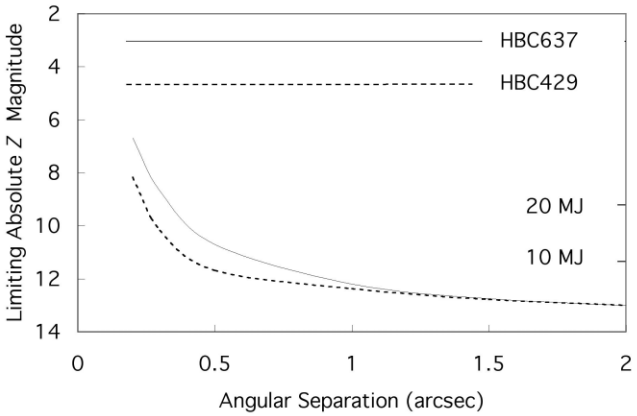

FIG. 4.—Absolute Z-magnitude detection limits for HBC 637 (*upper curve*) and HBC 429 (*lower curve*). The absolute magnitudes for objects with masses of $10M_J$ and $20M_J$ and ages of 3 Myr are labeled.

probably a background star. This interpretation is not inconsistent with the 2MASS photometry.

ScoPMS 21/5 is identified in the USNO-B1.0 and is also too faint to appear in the 2MASS catalog. The $B2$ value reported in the USNO-B1.0 is a couple of magnitudes brighter than our Z magnitude, suggesting that this is not a cool substellar object.

ScoPMS 21/7 is identified in the 2MASS catalog. The J and H magnitudes are flagged as upper limit nondetections, and K is flagged as background contaminated. ScoPMS 21/7 is also identified in the USNO-B1.0. The photographic colors together with our Z magnitude suggest a K star, but this object is too faint to be at the distance of the Ophiuchus star-forming region. This interpretation is not inconsistent with the 2MASS photometry.

HBC 633/1 is the relatively bright object only 3.″41 away from HBC 633. It is identified in the 2MASS catalog, but the photometry is unreliable because of its proximity to HBC 633. The separation is almost as small as the nominal 2MASS resolution of about 2.″6 FWHM. HBC 633/1 shows a slightly asymmetrical profile that is consistent with a binary composed of two similar components at a separation of about 0.″05 and a position angle of $179^\circ \pm 5^\circ$. HBC 633 itself is a close binary with a separation of about 0.″2 and K magnitude difference of 1.5 (Ghez et al. 1993). We do see a hint of an asymmetry in our subtracted image for HBC 633 at a position angle of roughly 160°, consistent with the value of 164° reported by Ghez et al. (1993). If HBC 633/1 is physically associated with HBC 633, then this system is at least quadruple.

Nine of our faint nearby objects have no matches in the USNO-B1.0 or 2MASS catalogs. To escape detection by the USNO-B1.0, they must be very red. On the other hand, to escape detection by 2MASS, the color cannot be too red. The limits depend on the observed Z value. For example, for ScoPMS 21/1 to escape 2MASS detection, its $Z - K$ color cannot be redder than about 1.7 mag. The Burrows et al. (1997) models predict that young substellar objects are almost always redder than $Z - K = 1.7$. Thus, ScoPMS 21/1 is unlikely to be a free-floating young object. A similar conclusion applies to ScoPMS 21/3 and HBC 633/2.

Thus, there is no compelling evidence that any of our faint nearby objects are substellar companions to our target stars. However, seven of our faint nearby objects (when HBC 391/1 is included) remain as candidate young substellar objects.

4. DETECTION LIMITS FOR FAINT NEARBY OBJECTS

We used simulated images to evaluate the limiting magnitude for the detection of a faint nearby object as a function of angular separation from its primary star. Artificial nearby objects were injected into real images for appropriate ranges in separation and brightness. The artificial nearby objects were generated by scaling the image of HBC 400. We searched our simulated images for detectable nearby objects in the same way as the real images. At separations larger than about 1″ the limiting apparent magnitude for the detection of faint nearby objects is about $Z = 19.5$ mag, independent of the brightness of the target. At smaller separations the brightness of the primary star becomes the dominating factor, and the detection limit depends on its brightness. This is illustrated in Figure 4, where the upper curve is the result of our simulations for HBC 637, absolute $Z = 3.15$ mag, and the lower curve is for HBC 429, absolute $Z = 4.49$ mag. For small separations the two curves have the same shape and are simply separated by the magnitude difference between the two stars. All of our other targets are brighter than HBC 429, so the lower curve represents our best performance. For our simulations we oriented our artificial objects so that they were located halfway between the diffraction spikes. Near the diffraction spikes our detection limit degrades by as much as a magnitude, and even more for very small separations. Inside a radius of about 0.″2, the subtracted images show residual instrumental speckles that are brighter than any possible substellar companions, so we did not try to simulate separations smaller than that. Our limiting detectable magnitude difference as a function of separation over the range 0.″2–1″ is similar to that reported by Sartoretti et al. (1998). We chose to plot absolute (instead of apparent) Z magnitudes in Figure 4 (assuming a distance of 150 pc) to make it easier to compare our detection limits with theoretical models. As an example, we indicate the absolute Z magnitudes for objects with masses of $10M_J$ and $20M_J$ and ages of 3 Myr in Figure 4.

We estimated the masses and ages of each of our targets for the luminosities and effective temperatures reported in Table 1 using four different sets of models for pre–main-sequence stars: D'Antona & Mazzitelli (1997, hereafter DM97), Baraffe et al. (1998, hereafter B98), Palla & Stahler (1999, hereafter PS99), and SDF00. The results are reported in Table 10 and show the well-known trend for the DM97 models to predict younger ages

TABLE 10
Mass and Age Estimates

	B98		PS99		SDF00			DM97		
Star	log t	M	log t	M	log t	M	M_p	log t	M	M_p
HBC 374	5.8	0.8	6.0	0.8	6.1	0.7	3	5.5	0.4	1
HBC 376	6.8	0.9	6.7	0.8	6.9	0.8	7	6.5	0.7	4
HBC 397	6.6	0.8	6.5	0.8	6.7	0.8	5	6.4	0.6	4
HBC 399	6.2	0.8	6.4	0.9	6.3	0.7	3	6.0	0.5	2
HBC 400a	6.7	0.9	6.7	0.8	6.8	0.8	6	6.4	0.6	4
HBC 400b	6.9	0.9	6.8	0.8	6.9	0.8	7	6.5	0.7	4
HBC 419	6.5	1.1	6.7	1.2	6.7	1.1	5	6.2	0.7	3
HBC 426	7.0	1.3	7.0	1.3	7.2	1.3	11	6.8	1.4	6
HBC 79	...	...	6.3	2.0	6.6	2.1	5	6.3	2.1	3
HBC 427	6.2	0.8	6.4	0.9	6.3	0.7	3	6.0	0.5	2
HBC 429	6.7	0.9	6.7	0.8	6.7	0.8	5	6.4	0.6	4
ScoPMS 21	7.2	1.2	7.4	1.1	7.3	1.1	12	7.0	1.2	8
HBC 630	...	...	6.8	1.3	6.8	1.5	6	6.3	1.3	3
HBC 633	7.1	1.2	7.2	1.2	7.3	1.2	12	6.9	1.3	7
HBC 636	6.5	0.7						6.1	0.7	
HBC 637			6.5	1.7	6.2	2.8	3	5.8	2.8	2

and smaller masses than the other three sets of models. In Table 10 the columns labeled log t give the target age in log years, and columns labeled M give the stellar mass in solar masses.

We then used our detection limit of apparent $Z \sim 19.5$ mag, corresponding to an absolute $Z \sim 13.6$ mag for an assumed distance of 150 pc, to estimate the limiting mass of any physical companion that we could detect. This limit applies to angular separations larger than about $1''$, for which the brightness of the primary is no longer important. We assumed that any physical companion would have the same age as its primary. For the expected thermal emission from a possible companion, we used the absolute Z magnitudes predicted by the evolutionary tracks for young substellar objects from Burrows et al. (1997). Adam Burrows kindly calculated for us the absolute Z magnitude for the *HST* W1042 passband as a function of age, as shown in Figure 5, so that we could use their evolutionary tracks. These limiting masses are reported in Table 10 for the DM97 and SDF00 models in the columns labeled M_p and are generally in the range of a few Jupiter masses.

5. DISCUSSION

For our Cycle 4 search for substellar companions with the PC2 (Sartoretti et al. 1998), we used the I band and a strategy of multiple exposures on a grid of nine spacecraft pointings before readout. For our Cycle 6 observations reported in this paper, we moved to the Z band, motivated by a new and better understanding of the spectra of very cool objects and the fact that their emission is dramatically higher than a blackbody in regions of low opacity, such as the Z band. To compensate for the much lower sensitivity of the PC2 in the Z band, we changed to a strategy of four exposures with 400 s of integration time each. This eliminated the heavy penalty of overhead time needed to point *HST* to a grid of positions in our Cycle 4 strategy, in effect converting that overhead into integration time. Although the limiting apparent magnitude for separations outside $1''$ was not as deep in Cycle 6, $Z \sim 19.5$ mag compared with $I \sim 21.5$ mag, the limiting detectable mass of a substellar companion was actually better than in Cycle 4. Because the effective wavelength of the Z band is about 20% longer than that of the I band, the PSF in the Z band is about 20% broader. However, this penalty against the detection of substellar companions close to the parent star is more than offset by the much better contrast between a cool companion and its hotter parent star in the Z band, typically a gain of about 2 mag, leading to a mass detection limit that was about a factor of 2 better in Cycle 6.

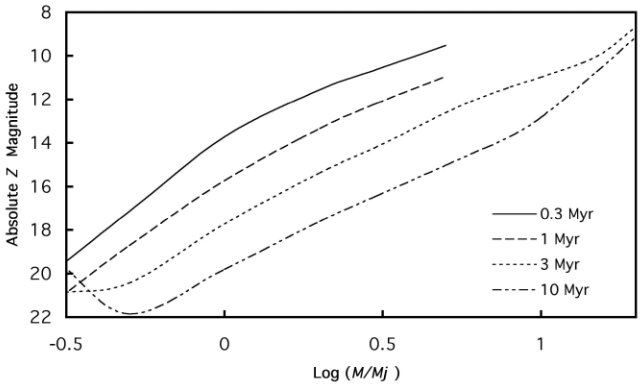

Fig. 5.—Absolute Z magnitude vs. mass as a function of age for the Burrows et al. (1997) models.

In the selection of targets for Cycle 6, we tried to identify the youngest weak-lined T Tauri stars that also met our other selection criteria. As a result the Cycle 6 targets are about a factor of 2 younger than the Cycle 4 sample. However, we did not realize this gain in the final ages adopted for our Cycle 6 targets, because we moved to the new generation of pre–main-sequence models, which tend to predict ages that are about a factor of 2 older than predicted by the DM97 models used for our Cycle 4 targets. Although the mass detection limits that we quote for our Cycle 6 observations in this paper do not look much better than the limits reported for Cycle 4, they are actually at least a factor of 2 better if the same models are used to estimate the ages.

Between the Cycle 4 and Cycle 6 projects, we have now probed for substellar companions around 24 WTTSs. At projected separations larger than about 500 AU (assuming a distance of 150 pc to the Taurus-Auriga and Ophiuchus star-forming regions), we have detected almost three dozen faint objects. Many of these have been detected in other surveys and can be explained as background stars, but a few of them lack the information needed to pinpoint their nature and could conceivably prove to be free-floating substellar members of their star-forming

regions. At separations smaller than 500 AU, we have detected several nearby objects but no substellar companions.

Previous surveys have led to the identification of four brown dwarf companions to young stellar objects at separations ranging from 100 to 250 AU: TWA-5B (Lowrance et al. 1999; Webb et al. 1999; Neuhäuser et al. 2000) with a separation of 110 AU and an estimated mass of about $20M_J$, HR 7329B (Lowrance et al. 2000; Guenther et al. 2001) at 200 AU and $40M_J$, GSC 08047-00232 (Chauvin et al. 2003, Neuhäuser & Guenther 2004) at about 250 AU and $25M_J$, and GG Tau Bb at 207 AU and $44M_J$. Based on the sample of 79 young stellar objects surveyed for the first three detections, Neuhäuser & Guenther (2004) estimate that the frequency of brown dwarf companions with separations larger than 50 AU is 6% ± 4%. Our PC2 images are sensitive enough to detect brown dwarfs over these separations, but we detected none. This null result by itself implies that the frequency of such brown dwarf companions must be less than 21% at the 3 σ level. Thus, there is weak evidence from the imaging surveys that the brown dwarf desert found by the Doppler surveys does not extend out past separations of 50 AU and stronger evidence that the desert does not extend out past 1000 AU (Gizis et al. 2001). At the present time little is known about the intermediate range, 5–50 AU.

Despite the low sensitivity of the PC2 in the *Z* band, we did gain about a factor of 2 in our mass detection limit compared with our earlier observations with the same instrument in the *I* band. Are there further gains to be won by moving further into the infrared, say, to the *J*, *H*, or *K* bands? We were surprised to discover that the *Z* band delivers better contrast than the longer bands for companions in the mass range $3M_J$–$10M_J$ and almost as good contrast for lower masses, on the basis of the predicted absolute magnitudes provided to us by A. Burrows. When the advantage of a narrower PSF at the *Z* band is taken into account, it looks like *Z* may prove to be the preferred band for the identification of candidate substellar companions at small separations. Of course, additional photometry in the longer bands can be critical for the interpretation of such candidates.

When we first started thinking about the detection of substellar companions around young stars more than 10 yr ago, not much was known about samples of young stars less distant than 150 pc. Recent work has disclosed several loose associations of moderately young stars, with a typical age of 10 Myr and at a typical distance of 50 pc. Although the older ages of these targets would degrade the mass detection limit, the closer distances would improve the limiting separation by a factor of about 3. Thus, young stars in these associations may merit deep high-resolution imaging in a search for substellar companions (Webb et al. 1999; Lowrance et al. 1999; Neuhäuser et al. 2002, 2003).

5.1. *Comments on Specific Targets*

5.1.1. *HD 283759*

In § 2.2.3 we presented compelling evidence that the radial velocity of HD 283759 excluded it from being a member of the Taurus-Auriga star-forming region. New proper motions from the UCAC catalog provide additional evidence that HD 283759 is not a member. Our other nine targets in Taurus-Auriga have a mean proper motion in right ascension of 5.4 mas yr^{-1} and rms deviations of 4.1 mas yr^{-1}. The corresponding proper motion of HD 283759 is 42.9 mas yr^{-1}, which differs by more than 9 σ.

5.1.2. *HBC 79 = SU Aur*

Our *Z*-band image of HBC 79 shows elongated nebulosity with an aspect ratio of roughly 2:1 oriented at a position angle of about 300°. The nebulosity is asymmetrical, extending mostly toward the west. It is clearly visible out to at least 5″ separation from the star.

We derived a temperature of 5523 K for HBC 79 by matching our observed echelle spectra with synthetic spectra calculated using Kurucz models. This is considerably cooler than the temperature of 5860 K that Kenyon & Hartmann (1995) report for this star on the basis of spectral type. A recent spectroscopic determination of the temperature of HBC 79 (DeWarf et al. 2003) yielded 5550 ± 100 K, very close to our result. This suggests that our spectroscopic effective temperature and surface gravity determinations may be better than the values derived from spectral types, even though our analysis technique was designed to optimize our radial velocities and not for the determination of fundamental astrophysical parameters. Our cooler temperature corresponds to an age that is a factor of 2 younger than the value listed in Table 10.

This example illustrates the difficulty of estimating reliable ages for young stellar objects. The uncertainties in the models are not the only problem. Observational uncertainties in the values derived for effective temperature and luminosity (which is sensitive to errors in the extinction and distance) can be just as important.

5.1.3. *HBC 400 = V826 Tau*

Previous work on the double-lined orbit of HBC 400 includes a definitive solution by Reipurth et al. (1990) based on CORAVEL observations. Our period of 3.887763 ± 0.000039 days is longer than their period of 3.887758 ± 0.000061 days by only 0.000005 days, well within the errors. Our period error is somewhat better, presumably because of the fact that our time coverage is more than twice as long. Reipurth et al. (1990) found that the spectral lines of one of the two stars appeared weaker in the composite spectrum by a factor of 0.69, presumably because the star was fainter. Our TODCOR analysis agrees that the same star is the fainter one and gives a light ratio of 0.75. Contrary to Reipurth et al. (1990), we find that the fainter star is also the less massive one, although the errors on our mass ratio are much too large for this result to be conclusive: $q = 0.997 \pm 0.032$. We did not assume a circular orbit but actually solved for the eccentricity. Our result, $e = 0.025 \pm 0.016$, is consistent with a circular orbit.

5.1.4. *HBC 427*

HBC 427 was first noted to be a spectroscopic binary by Mathieu et al. (1989) on the basis of velocities derived from 18 spectra obtained with the CfA Digital Speedometers. The span of the observations was only 1150 days, less than the orbital period of 2533 days, so no orbital solution was available. The single-lined orbit reported here is based on 58 CfA velocities spanning 5148 days. The tools that we now use to derive velocities have evolved significantly over the intervening years. For example, the use of synthetic template spectra allows us to match the observed spectra much better, and this has provided a significant improvement in the velocity errors, especially for stars that are rotating rapidly. Thus, the velocities reported here supersede those reported by Mathieu et al. (1989), even though some of them were derived from the same spectra. The dynamical masses for the two stars in the HBC 427 system were derived by Stefan et al. (2001), using the velocities reported here for the primary together with two velocities for the secondary derived from infrared spectra and an orbital inclination determined using the Fine Guidance Sensor 3 on *HST*.

We are indebted to Adam Burrows for supplying the absolute magnitudes from the models of substellar objects predicted by Burrows et al. 1997. Because most of the observations with the CfA Digital Speedometers are obtained under queue scheduling, many different observers contributed at the telescopes. We thank them all: Jim Peters, Perry Berlind, Bob Mathieu, Ed Horine, Bob Davis, Lee Hartmann, Mike Calkins, Robert Stefanik, Ale Milone, Joe Caruso, Larry Marschall, Joe Zajac, Ken Croswell, and Adam Leroy. As always, we thank Bob Davis for managing the database of observations from the CfA Digital Speedometers. Finally, we thank the anonymous referee for a very careful and thorough reading of our manuscript. Because of the many good inputs from the referee, this paper was improved significantly.

REFERENCES

Baraffe, I., Chabrier, G., Allard, F., & Hauschildt, P. 1998, A&A, 337, 403 (B98)
Bontemps, S., et al. 2001, A&A, 372, 173
Bouvier, J., & Appenzeller, I. 1992, A&AS, 92, 481
Burrows, A., et al. 1997, ApJ, 491, 856
Chauvin, G., et al. 2003, A&A, 404, 157
Chen, H., Myers, P. C., Ladd, E. F., & Wood, D. O. S. 1995, ApJ, 445, 377
Cox, A. N., ed. 2000, Allen's Astrophysical Quantities (4th ed; New York: AIP Press)
D'Antona, F., & Mazzitelli, I. 1997, Mem. Soc. Astron. Italiana, 68, 807 (DM97)
DeWarf, L. E., Sepinsky, J. F., Guinan, E. F., Ribas, I., & Nadalin, I. 2003, ApJ, 590, 357
Fitzpatrick, E. L. 1999, PASP, 111, 63
Ghez, A. M., Neugebauer, G., & Matthews, K. 1993, AJ, 106, 2005
Gizis, J. E., Kirkpatrick, J. D., Burgasser, A., Reid, I. N., Monet, D. G., Liebert, J., & Wilson, J. C. 2001, ApJ, 551, L163
Guenther, E. W., Neuhäuser, R., Huélamo, N., Brandner, W., & Alves, J. 2001, A&A, 365, 514
Hartmann, L., Hewett, R., Stahler, S., & Mathieu, R. D. 1986, ApJ, 309, 275
Hartmann, L. W., Soderblom, D. R., & Stauffer, J. R. 1987, AJ, 93, 907
Jones, B. F., & Herbig, G. H. 1979, AJ, 84, 1872
Kenyon, S., & Hartmann, L. 1995, ApJS, 101, 117
Kurtz, M. J., & Mink, D. J. 1998, PASP, 110, 934
Latham, D. W. 1985, in IAU Colloq. 88, Stellar Radial Velocities, ed. A. G. D. Philip & D. W. Latham (Schenectady: L. Davis Press), 21
———. 1992, in IAU Colloq. 135, Complementary Approaches to Binary and Multiple Star Research, ed. H. McAlister & W. Hartkopf (ASP Conf. Ser. 32; San Francisco: ASP), 110
Latham, D. W., Stefanik, R. P., Torres, G., Davis, R. J., Mazeh, T., Carney, B. W., Laird, J. B., & Morse, J. A. 2002, AJ, 124, 1144
Leinert, C., Zinnecker, H., Weitzel, N., Christou, J., Ridgway, S. T., Jameson, R., Haas, M., & Lenzen, R. 1993, A&A, 278, 129
Lowrance, P. J., et al. 1999, ApJ, 512, L69
———. 2000, ApJ, 541, 390
Mathieu, R. D., Walter, F. M., & Myers, P. C. 1989, AJ, 98, 987
Monet, D. G., et al. 2003, AJ, 125, 984
Neuhäuser, R., & Guenther, E. W. 2004, A&A, 420, 647
Neuhäuser, R., Guenther, E. W., Alves, J., Huélamo, N., Ott, T., & Eckart, A. 2003, Astron. Nachr., 324, 535
Neuhäuser, R., Guenther, E. W., Mugrauer, M., Ott, T., & Eckart, A. 2002, A&A, 395, 877
Neuhäuser, R., Guenther, E. W., Petr, M. G., Brandner, W., Huélamo, N., & Alves, J. 2000, A&A, 360, L39
Nordström, B., Latham, D. W., Morse, J. A., Milone, A. A. E., Kurucz, R. L., Andersen, J., & Stefanik, R. P. 1994, A&A, 287, 338
Nürnberger, D., Brandner, W., Yorke, H. W., & Zinnecker, H. 1998, A&A, 330, 549
Oppenheimer, B. R., Kulkarni, S. R., Matthews, K., & van Kerkwijk, M. H. 1998, ApJ, 502, 932
Palla, F., & Stahler, S. W. 1999, ApJ, 525, 772 (PS99)
Reipurth, B., Lindgren, H., Nordström, B., & Mayor, M. 1990, A&A, 235, 197
Reipurth, B., & Zinnecker, H. 1993, A&A, 278, 81
Richichi, A., Leinert, C., Lameson, R., & Zinnecker, H. 1994, A&A, 287, 145
Sartoretti, P., Brown, R. A., Latham, D. W., & Torres, G. 1998, A&A, 334, 592
Seiss, L., Dufour, E., & Forestini, M. 2000, A&A, 358, 593 (SDF00)
Simon, M., et al. 1995, ApJ, 443, 625
Stefan, A. T., et al. 2001, AJ, 122, 997
Strom, K. M., Strom, S. E., Edwards, S., Cabrit, S., & Skrutskie, M. F. 1989, AJ, 97, 1451
Sudarsky, D., Burrows, A., & Hubeny, I. 2003, ApJ, 588, 1121
Wachter, S., Hoard, D. W., Hansen, K. H., Wilcox, R. E., Taylor, H. M., & Finkelstein, S. L. 2003, ApJ, 586, 1356
Walter, F. M., Brown, A., Mathieu, R. D., Myers, P. C., & Vrba, F. J. 1988, AJ, 96, 297
Walter, F. M., Vrba, F. J., Mathieu, R. D., Brown, A., & Myers, P. C. 1994, AJ, 107, 692
Webb, R. A., Zuckerman, B., Platais, I., Patience, J., White, R. J., Schwartz, M. J., & McCarthy, C. 1999, ApJ, 512, L63
Zucker, S., & Mazeh, T. 1994, ApJ, 420, 806